SSRG International Journal of Mechanical Engineering
ISSN: 2348-8360/ https://doi.org/10.14445/23488360/IJME-V11I7P102

Volume 11 Issue 7, 13-25, July 2024

Original Article

A Tribological Study of Antimony-Impregnated Graphite for Steam Mechanical Seals

Lathesh Madhavan[1], Rahul Waikar[2], Abhijeet Deshpande[1]

[1]*Research and Development Department, Forbes Marshall Pvt. Ltd., Maharashtra, India.*
[2]*Industrial and Production Engineering Department, Vishwakarma Institute of Technology, Maharashtra, India.*

[1]*Corresponding Author : latheshmadhavan@yahoo.com*

Received: 04 May 2024 Revised: 05 June 2024 Accepted: 03 July 2024 Published: 30 July 2024

Abstract *- Wear resistance, self-lubrication, and chemical stability of Antimony-Impregnated Graphite (AIG) grades in steam environments make them suitable for mechanical sealing requirements in Rotary Unions in paper manufacturing industries. The working conditions of such seals had been re-created in pin-on-disc tests, and the tribological characteristics were studied. Pins made of three commercial grades of AIG had been tested against Grade 304 Austenitic stainless-steel discs. Pin-on Disc wear tests in constant loading and time-dependent loading conditions were conducted in pressurized steam environments. Scanning Electron Microscopy, EDX, Raman Spectroscopy, and wear track profiles were analyzed on samples. The wear rate of the pins had increased with an increase in load up to a specific limit. Raising the load further caused the stage-wise failure of the transfer film. This resulted in the wear of the metal surface and a reduction in pin wear. This observation corroborated with the components obtained from industrial installations. Sinusoidal loading resulted in microcracks on the loaded surface and rupture of many samples. The wear rate was observed to be reduced due to a much more stable transfer layer.*

Keywords *- Antimony-Impregnated Graphite (AIG), Lubrication, Mechanical seals, Tribology, Wear resistance.*

1. Introduction

In the past decade, research in the tribological properties of AIG has gained momentum due to its applicability in motors, mechanical sealing, and self-lubricated bushing applications. The present study offers some insight into the mechanisms of wear and failures observed in steam-based mechanical sealing systems used in Rotary Unions (RU) in the paper industry. Any failure in the seals results in the downtime of the whole paper dryer section, loss of steam generated, production losses, and safety issues due to leakage of high-temperature steam. Past studies have explored the compositions of AIG, manufacturing process, effects of these on tribology [1], and advantages over other graphites [2] in dry sliding tests. However, the base mechanisms involved in graphite lubrication were explored in [3-5]. Zaidi et al. [3] studied the transition Coefficient of Friction (COF) of graphite crystallites through 3 states, i.e., α, β, and γ, with COFs 0.1, 0.3, and up to 0.6, respectively. Studies on Al-Si alloy-impregnated graphite composites [6] in moist environments showed an increasing trend in wear rate at lower loads and then a decrease at higher loads. The studies on Raman spectroscopy of graphite materials [7, 8] and impregnated graphites [2] undergoing wear revealed that the intensity ratio of the D peak at 1350 cm-1 to the G peak at 1580 cm-1, denoted as ID/IG, was proportional to the degree of disorder in the microstructure. In wear studies with time-dependent loads [9-12], the increased friction and vibration amplitude reduced the friction coefficient for various alternate materials [9, 10]. In PTFE, the wear rates observed during variable loading conditions were more than those at the mean static loading conditions [11, 12]. The wear rates also increased with an increase in dynamic loading constant. Detailed research in learning time-dependent loading in the live application and recreating the loading conditions in tribological testing was observed in dental and prosthetics research [13-17].

In application-specific research in mechanical face seals, secondary seals, and guides made of AIG used in RUs [18-22], the effect of transfer layers and balance ratios on the performance of RUs was studied. In our previous work, a comprehensive study was carried out on the loads experienced by a mechanical seal assembled into a similar RU in static, dynamic, and unbalanced loading conditions using strain gauges mounted on the seal and by frictional Torque measurement. The RUs studied were with stainless steel covers. In Table 1, the static loads to be applied in Pin on Disc tests on a 10 mm diameter pin, calculated from strain gauge readings and validated by Finite Element Analysis (FEA), at various media pressures during these tests are replicated.

Table 1. Dead weights are to be applied on pins evaluated for static load tests

Air Pressure in Mpa	Maximum Contact Pressure Mpa	Maximum Contact Pressure (Pa)	Average Load on Pin (N)	Average Load on Pin (kg)	Dead Weights (g)
0.1	0.362	361710	28.409	2.90	2920
0.2	0.617	616600	48.428	4.94	4910
0.3	0.870	870350	68.357	6.97	6900
0.4	1.123	1123000	88.200	8.99	8900
0.5	1.375	1374700	107.969	11.01	10900

Table 2. Load parameters for sinusoidal load tests

Config. No	Load Configuration	Limit	Contact Pressure (Mpa)	Loads on Pin (N)	Mean Load (N)	Frequency (Hz)	Dynamic Constant [6]
1	From stretched Hose Load Tests and FEA	Upper Limit	0.94	73.8	59.7	1.5	1.62
		Lower Limit	0.58	45.6			
2	From Frictional Torque Tests- 2mm Misalignment	The Upper Limit from 25 Nm	0.669	52.5	36.8	3	2.5
		Lower Limit from 10Nm	0.268	21.05			
3	From Frictional Torque Tests, mm Misalignment	The Upper Limit from 25 Nm	0.669	52.5	42	1.5	1.67
		Lower Limit from 15Nm	0.401	31.5			

Table 3. Properties of AIG pins

Material	Density (kg/m3)	Shore Hardness	Hardness HRB	Compressive Strength (MPa)	Flexural Strength (MPa)	Coefficient of Thermal Expansion ($10^{-6}C^{-1}$)
Grade A	2500	80	102, 101, 99, 105	276	90	4.7
Grade B	2300	-	99, 103, 86,43	250	80	4.2
Grade C	2250	-	102, 89, 101, 90	350	90	4.5

Table 2 shows the parameters for time-dependent, approximated sinusoidal loads to be applied on the pins, evaluated by combining fractional torque measurement, strain gauge measurement, and FEA techniques; the seal experiences these dynamic loads due to improper installations like stretched connection hoses or misalignment. An additional column for dynamic load constant, as discussed by Patil et al. [12, 13], has been calculated and added to the results.

In the present study, a wear testing machine shown in Figure 1 with sinusoidal loading capability and steam environment was designed and fabricated to conduct tests based on parameters in Tables 1 and 2. Pins of 10mm diameter and 30mm length made of a commercial grade AIG (mentioned as grade A) were tested by sliding over grade 304 austenitic stainless-steel discs. A torque sensor is used to obtain frictional torque. The other end of the torque sensor was assembled to a 3HP 3-phase motor controlled by a Variable Frequency Drive (VFD). Dead weights were directly applied on a pin holder to achieve static load values, as mentioned in Table 1, on the pins. A scotch yoke mechanism with a stroke length of 40mm, used to compress a spring housed in a spring guide, was assembled onto the dead weights. The shaft of the scotch yoke mechanism was connected to a single-phase induction motor controlled by another VFD. The load applied by this system is mentioned in Table 2. Three separate springs were designed to obtain the three different amplitudes of loads.

This loading system was enclosed in a chamber that maintained a high-pressure steam environment. The steam circuit additionally had a boiler with 1 ton per hour capacity, an accumulator, a pressure-reducing valve, etc., at the inlet to the chamber, and a steam trap at the condensate outlet. A thin film temperature sensor was used to ensure the steam was saturated near the pin. The tribological characteristics of 3 different commercial grades of AIG, henceforth mentioned as grades A, B, and C, were tested on this machine and compared in this study.

2. Materials and Methods

Table 3 gives the properties of grades A, B, and C. HRB hardness was measured at four locations in the samples. Both Grade A and C exhibited hardness values in the range of 89 to 105. In grade B, the range was observed to vary between 43 and 103. The detailed composition of each material is not discussed due to patent and confidentiality infringement issues.

The stainless-steel discs were machined to 150 mm diameter and 5 mm thickness. The surface roughness was maintained between 0.45 and 0.65 Ra values. Rockwell HRB hardness was observed in the range of 80 to 90. The mean diameter of the wear track was decided to be taken as 110 mm. Tests 1, 2, and 3, described below, were conducted on the test specimens.

2.1. Test 1: Wear Tests with Static Loads

Due to the high expenditure in conducting the tests, the number of static load tests conducted was limited to the test parameters mentioned below. Testing was done by maintaining 0.4 MPa steam pressure, 22500 revolutions of the wear disc measured using a cycle counter (i.e., for 7775 m of rubbing distance), and at 461 mm/s sliding velocity.

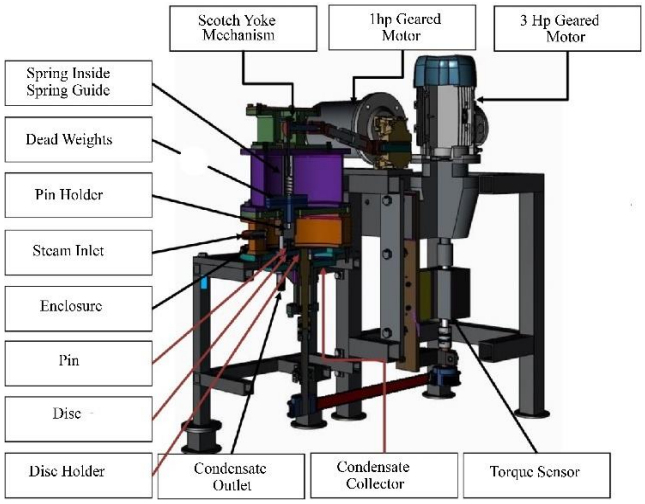

Fig. 1 Schematic of wear testing machine with sinusoidal loading capability and steam enclosure

Two pins of each material were tested at the five loads mentioned in Table 1. Weights of the pins before and after testing were measured using a Mettler Toledo AX-26 weighing scale, which has a resolution of 0.02mg. The wear rate of the sliding distance in mg/meter was evaluated. Before weighing, the pins were kept in a furnace at 120° C for 1 hour to remove the adsorbed moisture. The frictional torque measured was recorded in a data acquisition system, from which the coefficient of friction Vs time plots were prepared. The wear track profile tracks were traced using a Mitutoyo RA-2200 surface profile tester. Selected samples of the disc were observed under an optical microscope for macroscopic observations and SEM for microstructure study. EDX analysis was also done on selected specimens.

2.2. Test 2: Wear Tests with Sinusoidal Loads

Two pins for each of the three grades of AIG were tested at the same operating parameters, except that sinusoidal loads as per parameters mentioned in Table 2 were applied. The measured wear rates were compared to those evaluated when mean loads of these sinusoidal patterns were to be applied in static load tests, Raman Spectroscopy was done on selected pins to study surface changes.

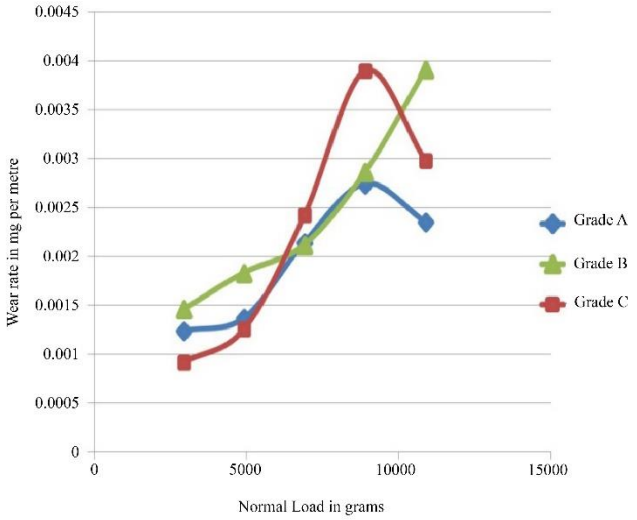

Fig. 2 Wear tests on three samples of different grades by varying load

3. Results and Discussion

Figure 2 shows the average wear rates in mg/m of sliding distance for the three grades measured during the test. For grades A and C, it was observed that wear rates and the slope of the curves increased with an increase in normal loads until a load of 6900g was reached. After that, the slope of the curves started reducing, and beyond 8900g, the wear rates started reducing. For grade B, the wear rate showed an increasing trend throughout the range of the tests. Detailed evaluation of each stage of the wear regime in the graph is discussed below in corroboration with other lab results.

3.1. 2920 g and 4910 g Loading Conditions

The SEM images taken at 100X magnification of the Transfer Layers (TL) observed on the disc for 4910g load for grades A, B, and C materials are shown in Figures 3(A), 3(B), and 3(C). All three materials show almost evenly dispersed TLs at a 4920g load. TL of grade B was seen to have a paste-like consistency, grade C had a watercolour-like texture, and on grade A, the TL was powdery. Comparing optical microscope images in Figure 4(A) with Figure 4(C) and 4(D), it may be observed that the TL had got evenly filled inside the machining marks for grades A and C, and a stable interfacial lubricant layer was formed at 4950g load. The

powdery nature of TL of grade A and the watercolour-like nature of grade C are visible in Figures 4(C) and 4(D), respectively. Figure 5 shows the profiles of wear tracks formed by the three grades of pins on the disc. The wear depth observed for grades A, B, and C at 2920g and 4910 g was only near 2 to 3 microns. Even when the test was prolonged to 15000m for a 4910 g load, neither the overall pin wear loss nor the wear track depth was observed to increase significantly, i.e., Once a stable TL was formed at these loads, it protected the mating components from getting into an aggressive wear mode. The 2- 3 microns of disc wear occurred during the initial run-in period, where the TL formation was still in progress. Figure 6 shows the plots for the Coefficient of Friction (COF) Vs time observed during test 1. The COF stabilizes at values much lower than 0.2 for 2920g and 4910g loads for all three materials. It may be inferred that α regime [3] of wear exists between 2920 and 4910 g loads.

The Raman Spectroscopy done on worn surfaces of the pin specimens is shown in Figure 7. The columns in Figure 7 show the spectra for unworn specimens, specimens worn at 4920g load, and specimens worn at three configurations of sinusoidal load tests. The three rows are for pin materials A, B, and C. Comparing the first two columns, it may be observed that the ID/ IG ratio reduces when a pin is subjected to a 4920g load in a wear test, showing that some degree of organizing of microstructure occurs during wear at these loading conditions, in the steam environment also, similar to dry wear tests in [2, 7, 8]. The EDX done on the disc specimens may be observed in Figure 8, and the corresponding numerical values of atomic percentage are in Table 4. Figures 8(A), 8(D), and 8(F) and the corresponding values in Table 4 show a significant presence of carbon layer on the surface for all the pins. The carbon percentage is highest for grade A, and the oxide formation is highest for grade C.

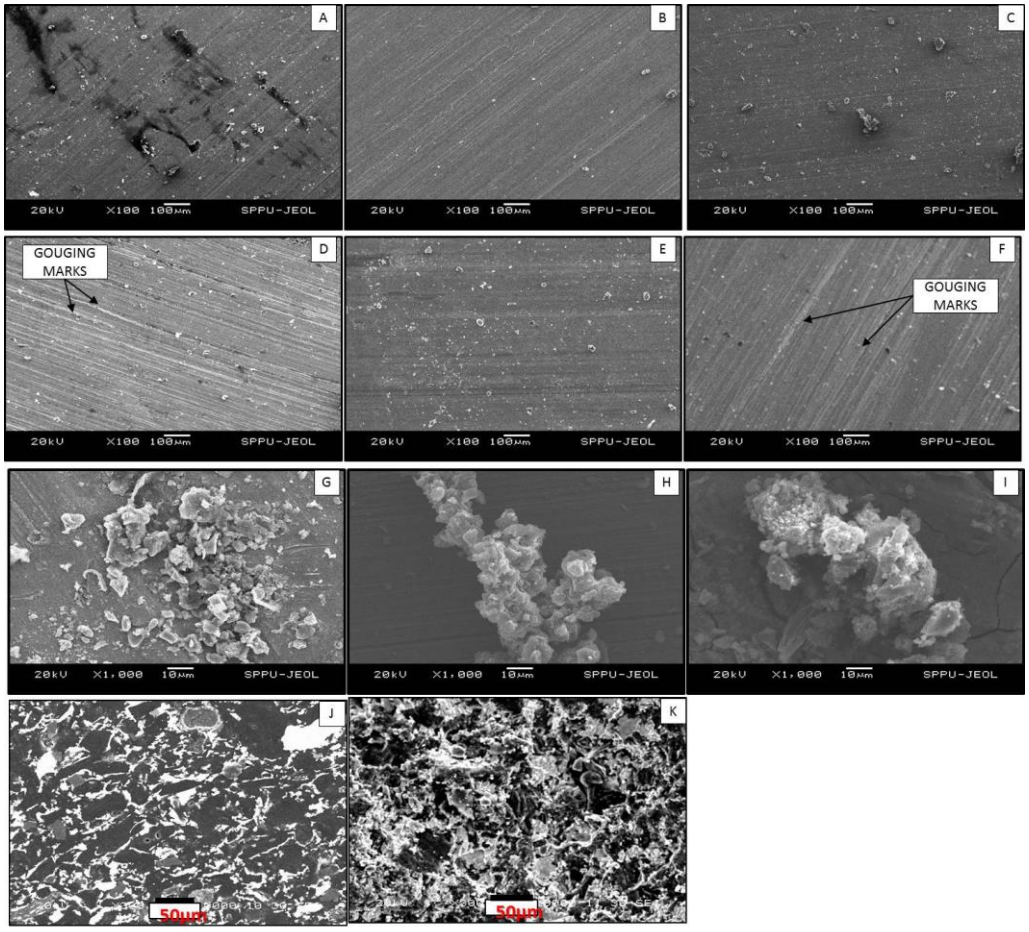

Fig. 3 SEM images (A), (B), (C) are taken at 100x of discs for pin materials A, B, and C at load 4920 g, (D), (E) and (F) are taken at 100x of discs for pins A, B, and C at load 6900 g, (G), (H) and (I) are taken at discontinuities of the transfer layer at 1000x of discs for pins A, B, and C at load 6900 g, (J) is taken of a general cross-section of grade B pin material and (K) is the SEM Image of the fractured surface of grade B material.

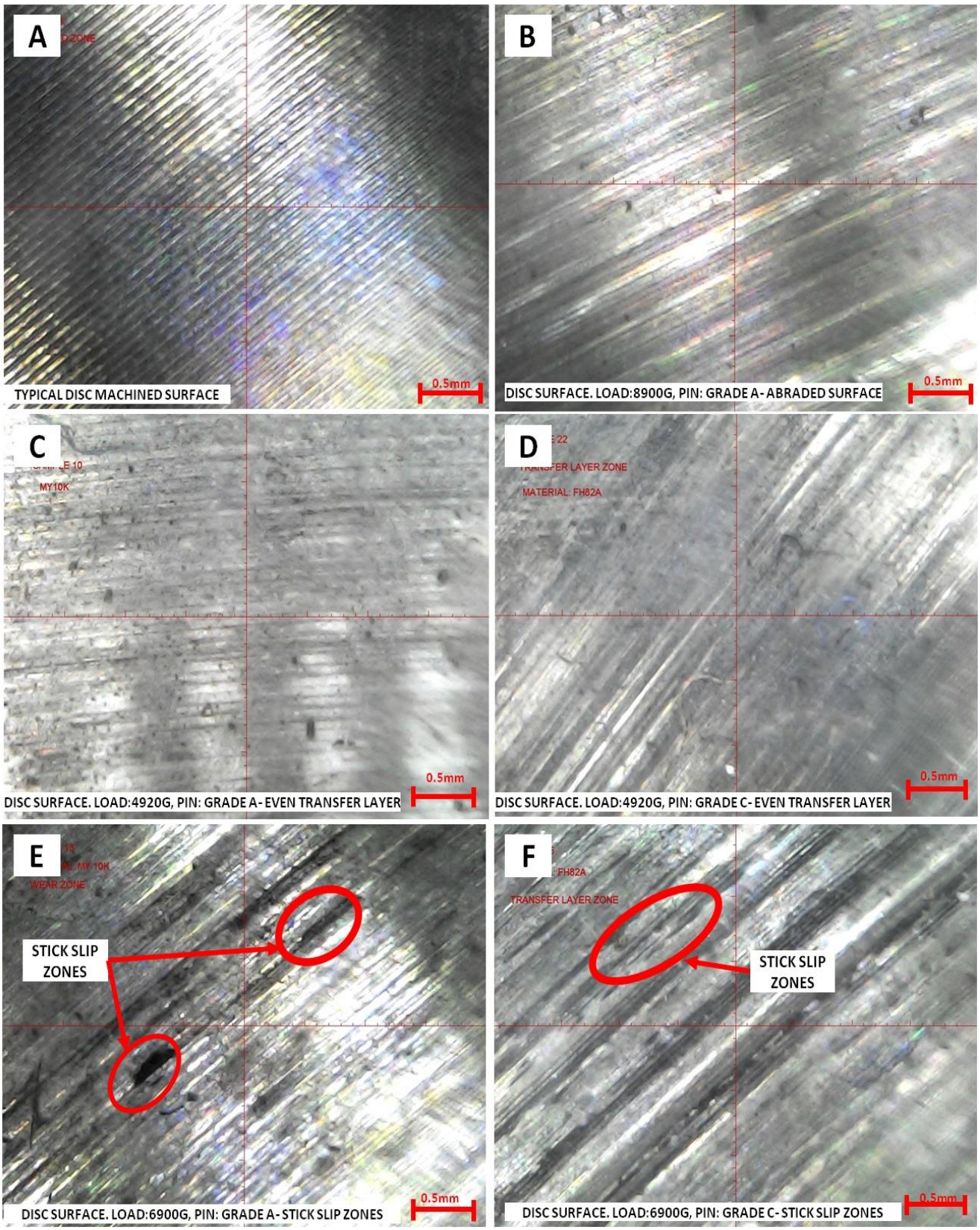

Fig. 4 Optical microscopic images of disc surfaces (A) Freshly machined disc surface, (B) Disc surface pin: grade A 8900 g load, (C) Disc surface pin: grade A 4920 g load, (D) Disc surface pin: grade C 4920 g load, (E) Disc surface pin: grade A, 6900 g load, and (F) Disc surface pin: grade C, 6900 g load.

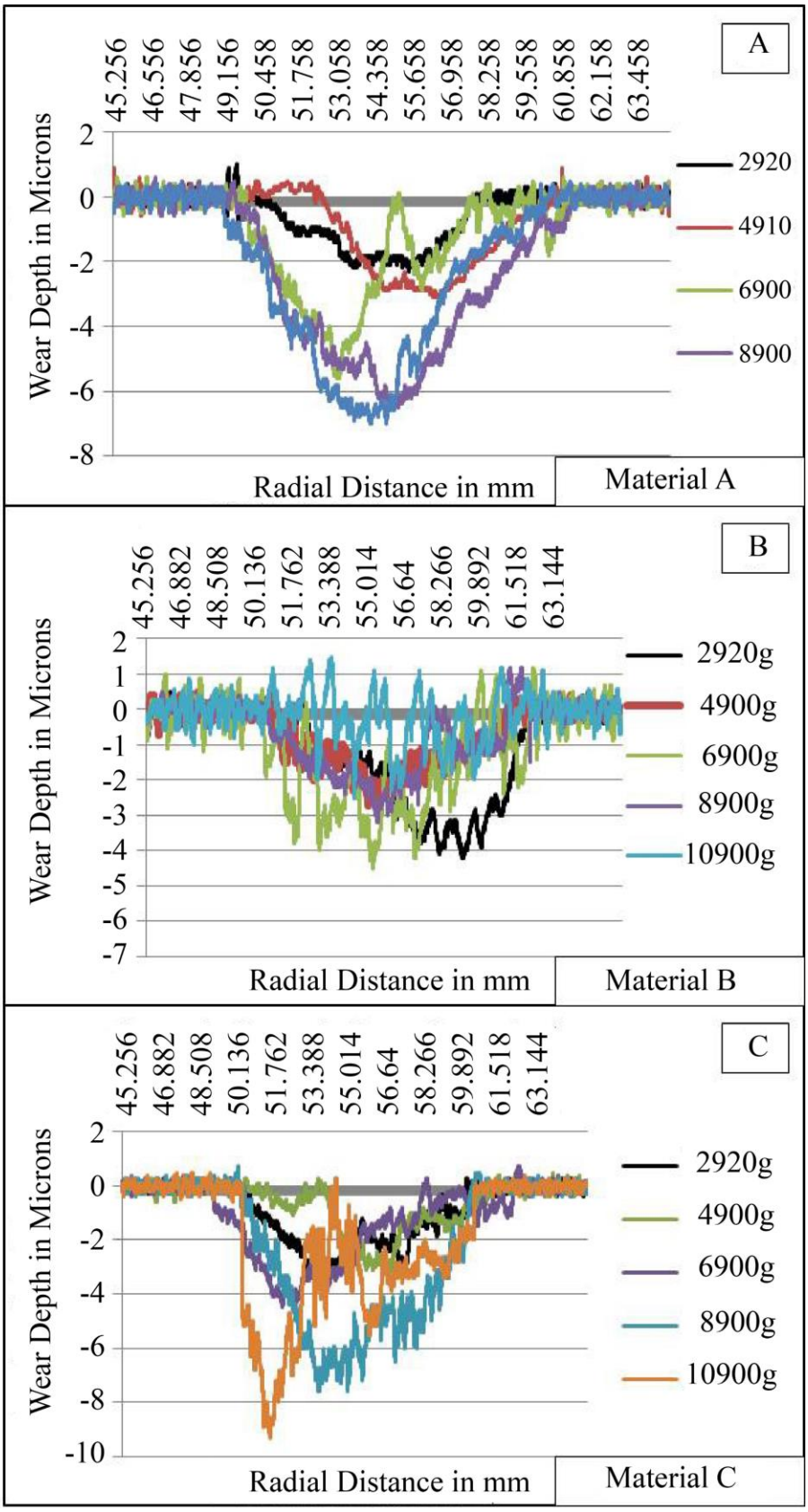

Fig. 5 Surface profiles of wear track for grades A, B, and C material for various static loads

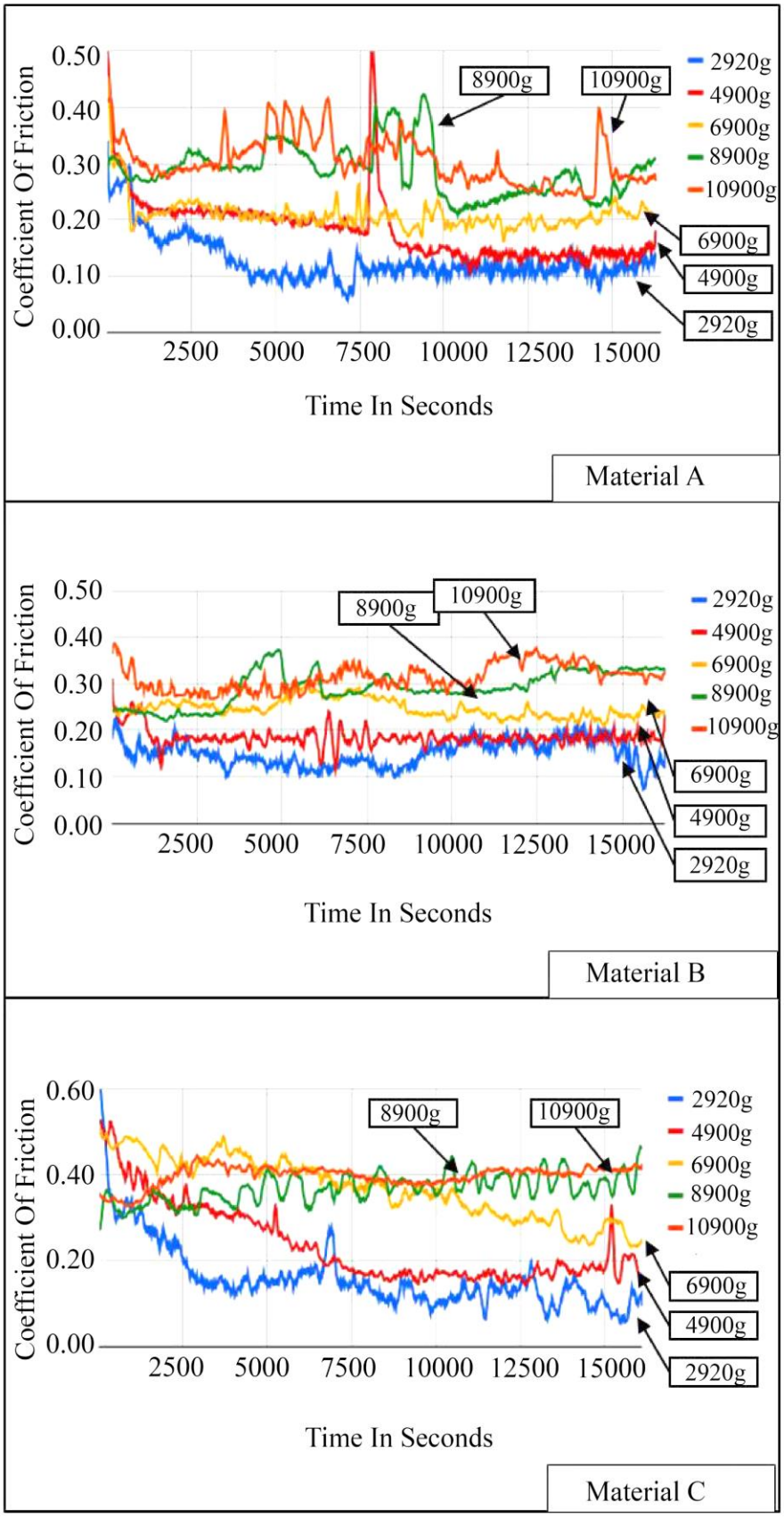

Fig. 6 Coefficient of friction vs time graphs during test 1

3.2. Test at 6900 g Load

Microscopic images of TL formed, shown in Figures 4(E) and 4(F), for grades A and C show patches indicating that a stick-slip phenomenon starts at this load. SEM Images 3D and 3F show gouging marks on the disc surfaces tested against grades A and C. The discontinuities in the TL, observed at 1000X in SEM, are shown in 3G, 3H, and 3I. The powdery nature of the TL of grade A is confirmed in Figure 3(G). 3(H) reveals the laminarity of the TL of grade B. In Figure 3(I), grade C shows a partially grainy and partially laminar texture. The results show that the TL formed disintegrates partially for grades A and C. In the zones where the TL gets removed, the portion of the disc surface gets exposed to the pin's bulk hardness, resulting in disc surface gouging. During hardness testing of pin specimens, the indenter of the tester ruptured several times, implying that the local hardness of localized areas on the AIG could go to much higher values than stainless steels. These zones should be capable of micro-cutting the steel surface if there is no protective solid lubricant surface between the pin and the disc. Hence, partial progressive wear occurs on the pin and disc. Discs tested against grade B were also observed to have a steady TL at 6900 g load. The friction coefficient plots for 6900 g stand apart from 2920 and 4910g in Figure 7 for all three grades, and they come closer to a value of 0.2 as time progresses.

3.3. Test at 8900 g and 10900 g Loads

When tested with grade A pins at 8900g load, the disc surface is shown in Figure 4(B). No transfer layer was observed. In-depth abrasion was seen on the disc. Compared with Figure 4(A), initial machining marks had been thoroughly abraded off. A similar nature was observed for grade C also. EDX given in Figure 9(C) and values given in column 4 of Table 4 confirm this observation by showing zero carbon percentage on the surface. Wear tracks shown in Figures 5(A) and 5(C) for 8900g and 10900g loads are significantly more profound than the rest. Hence, in this wear regime, it can be observed that the wear of the disc starts dominating over the wear of the pins when the more challenging pin encounters the softer disc. The coefficient of friction plot in Figure 6 for 8900g and 10900g for all three pins stand apart from all other loads and reach 0.3 or above in all the plots.

Figures 6(A) and 6(C) also show severe fluctuations due to the pure cutting action between the tribological pairs, fluctuating between β and γ regimes of friction. As the wear of the disc dominates over the wear of the pin, the pin wear rates are observed to come down for a 10900g load in Figure 2 for grades A and C. This increasing and decreasing trend of the wear rate Vs load curve for AIG in a steam environment can be very similar to the observation while testing Al-Si alloy-impregnated Graphite composites in moist environments [6].

However, grade B shows an increasing trend in Figure 2 concerning load. The transfer layer did not disintegrate even at higher loads. The wear tracks observed in Figure 5(B) were only within 4 microns, even for a 10900g load. The coefficient of friction is also observed to be lesser than the rest of the two materials.

Table 4. EDS results on plate surfaces tested against pins of A, B, and C materials at various loads

Pin material/ Loads Elements	Pin A/ 4920 g Atomic %	Pin A/6900 g Atomic %	Pin A/ 8900g Atomic%	Pin B/ 4920g Atomic %	Pin B/ 6900g Atomic %	Pin C/ 4920g Atomic %
C	61.66	48.07	0.00	47.95	48.79	50.13
O	21.30	29.75	52.31	24.80	29.27	37.30
Si	0.39	0.84	1.26	0.54	0.43	0.87
Cr	3.55	4.65	9.89	5.73	4.33	2.24
Mn	0.29	0.51	0.00	0.00	0.00	0.00
Fe	11.63	14.62	32.73	18.77	14.49	7.55
Ni	1.17	1.55	3.80	1.93	1.91	0.62
Sb	0.00	0.00	0.00	0.28	0.78	0.11

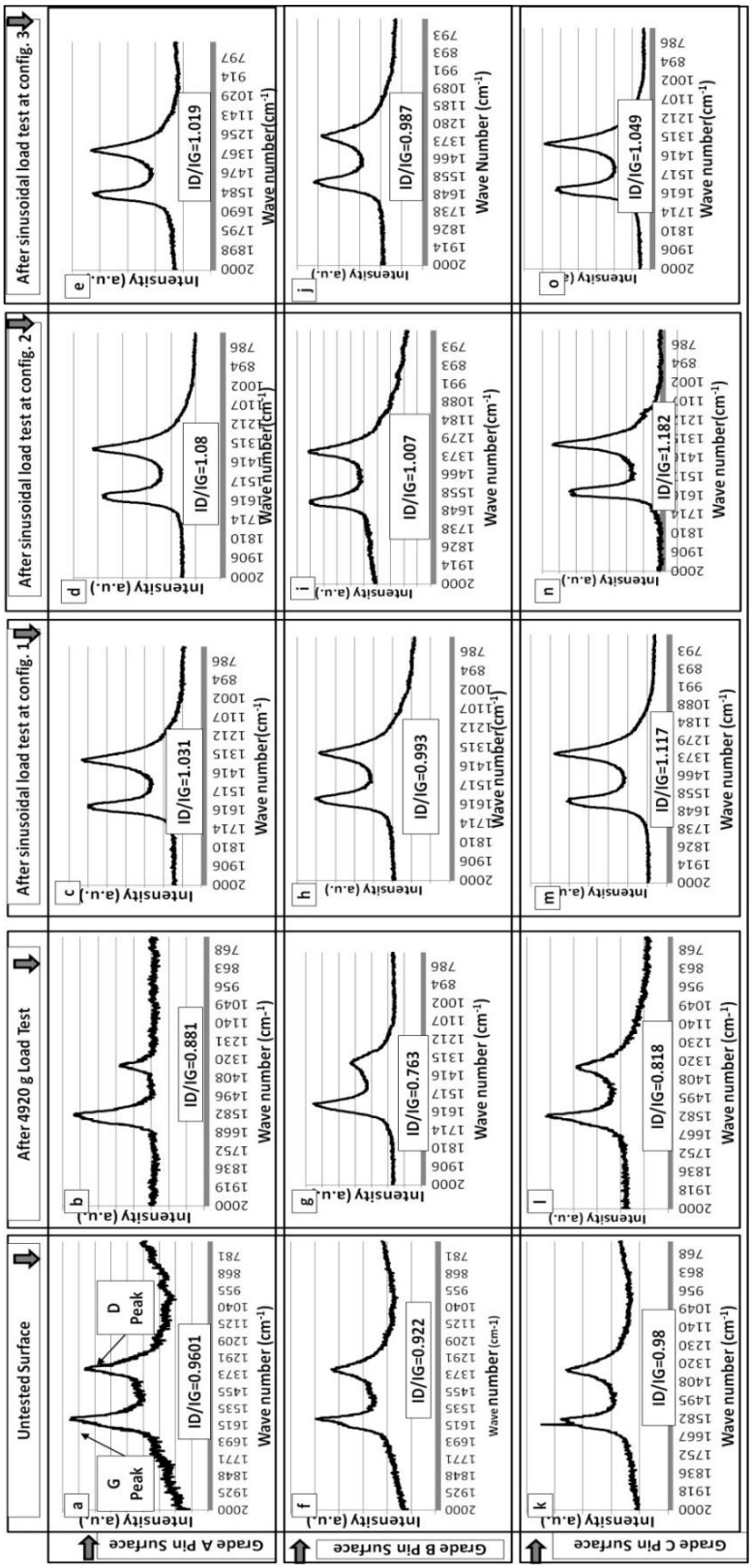

Fig. 7 (a), (b), (c), (d), (e) are Raman spectra for pin material A. (f), (g), (h), (i), (j) are for material B. (k), (l), (m), (n), (o) are for material C. Spectra in (a), (f), (k) are done for pin specimens before wear tests. Spectra in (b), (g), and (l) are used for constant load tests at 4920 g. Spectra in (c), (h), and (m) are for pins tested in configuration 1. (d), (i), and (n) are for pins tested in configuration 2. (e), (j), (o) are for pins tested in configuration 3 in sinusoidal load testing.

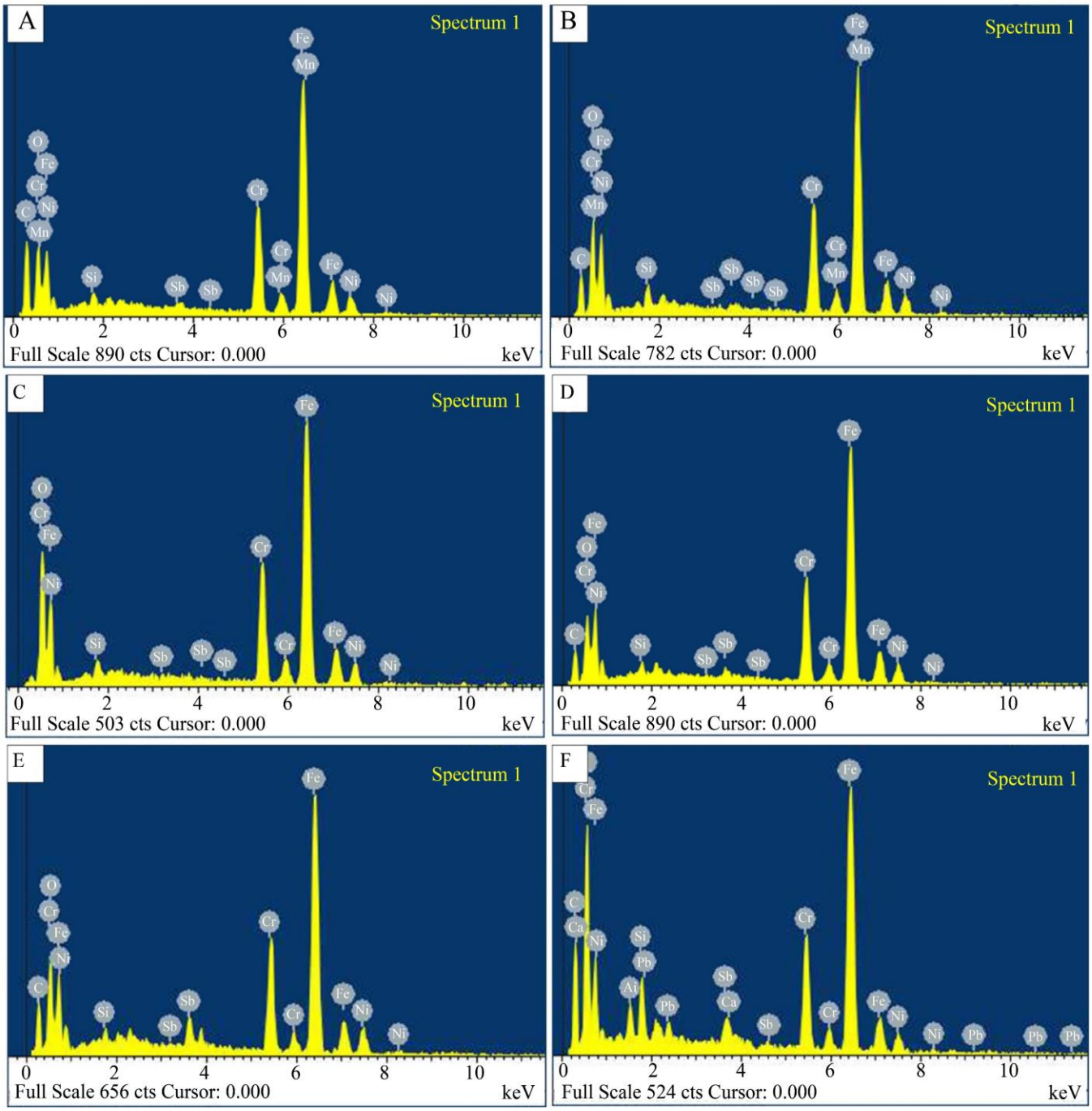

Fig. 8 EDX of disc surfaces (A) Load 4920 g pin: grade A, (B) Load 6900 g pin: grade A, (C) Load 8900 g pin: grade A, (D) Load 4920 g pin: grade B, (E) Load 6900 g pin: grade B, and (F) Load 4920 g pin: grade C.

3.4. Results of Test 2, Wear Testing with Sinusoidal Loading Arrangement

The wear rates obtained for grade A, B, and C pins for the three sinusoidal loading configurations are shown in Figures 9(A), (B), and (C), respectively. The mean value of each loading configuration, given in the sixth column of Table 2, is taken on the X-axis. The mean wear rate curve during static loading from Figure 2 is replicated in blue for reference. The range in which the sinusoidal load was applied concerning time for each load configuration is shown, with the maxima and minima of the loading curve as vertical dotted lines. The intersection points of a dotted line with the blue curve may be taken as the wear rate expected when a static load of the respective value of maxima or minima is applied in constant load tests. Hence, for grades A and B, the wear rates observed during sinusoidal loading were even

below the expected wear rates if a constant load with a minimum value of the sine curve was applied. This differs from the dynamic wear characteristics of PTFE [11, 12]. The third, fourth and fifth columns of Figure 7 show that disorder increases in AIG during test 2. High ID/IG ratios in column 5 imply that loading frequency has the most significant effect on surface disorder. Comparing columns 3 and 5, an increase in mean load also increases disorder when the dynamic constant is almost the same. An increase in wear with an increase in dynamic loading constant was also not evident. This could be because AIG forms a much more stable transfer layer than PTFE, which could absorb the load's dynamic effects.

The wear rates from sinusoidal tests were higher than the static tests, only in grade C. Though the wear rates for grade B were lower, the pin material cracked four times during the tests, so re-tests were conducted. Row 2 of Raman data in Figure 7 shows that material B has the maximum percentage change in ID/IG ratio during test 2, implying microcracks developed on the surface. Comparing SEM images of a regular cross-section of grade B material, given in Figure 3(J), with the image of a cracked surface, given in Figure 3(K), the abundance of white-coloured antimony on the fracture surface may be noticed. The fracture generated due to sinusoidal loading propagates through the antimony network within the crystal structure.

This mode of failure explains the failure of AIG seals, given in Figure 10(A), when utilized in RUs installed with misalignment and incorrect installation of hoses in the Paper Industry. Catastrophic wear in RU shafts in contact with these seals shown in Figure 10(B) could be due to excessive loading due to stretches hoses above contact pressures of 0.87 MPa, the value being taken from Table 1 or incorrect calculation of balance ratios of the seals [19]. Though the properties of grade B material were superior in static load tests, the material was observed to fail structurally during sinusoidally loaded wear tests. Amongst grades A and C, grade A was observed to have lower wear rates in static load wear tests.

3.5. Discussion

Based on the findings, it is clear that the wear behavior of the three grades varies significantly under different loading conditions. For grades A and C, as the load increased to 6900g, the wear rates and the curve slopes also increased. However, when the load exceeded 8900g, the wear rates decreased, indicating a stabilization effect. This effect is likely due to the formation of a protective Transfer Layer (TL) that reduces aggressive wear.

On the other hand, grade B consistently showed increasing wear rates, suggesting that it had less stability in forming a TL. Microscopic and spectroscopic analyses supported these observations, showing different TL textures and compositions for each grade. Grade A developed a powdery TL, while grade C formed a watercolour-like TL. The coefficient of friction stabilized below 0.2 for loads up to 4910g, indicating effective lubrication.

However, at higher loads (8900g and above), the wear mechanisms changed, leading to more pronounced abrasion and increased friction, especially for grades A and C. This change was not seen in grade B, which maintained a stable TL even at higher loads, showing different wear dynamics compared to the other grades.

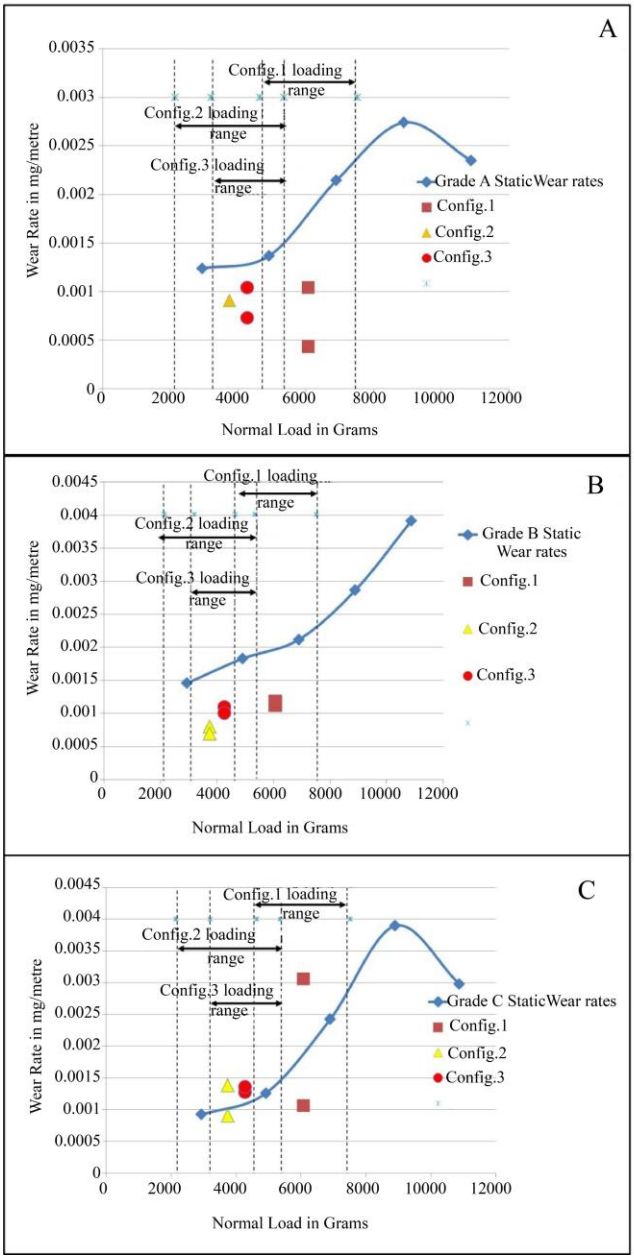

Fig. 9 Pin wear rates during sinusoidal loading conditions (A) is for grade A, (B) is for grade B, and (C) is for grade C.

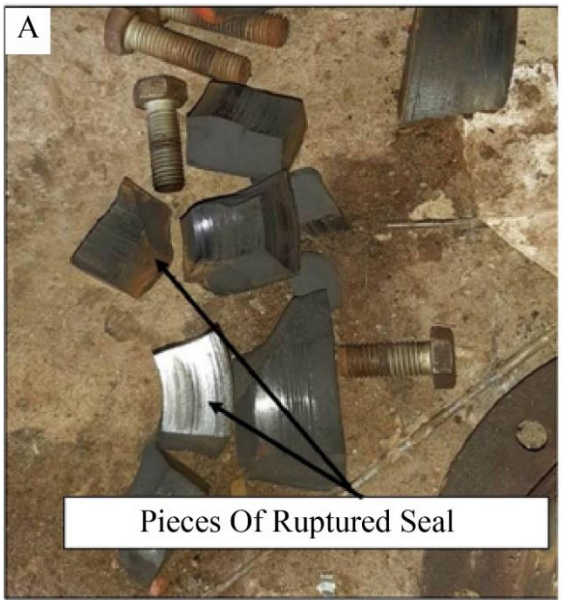

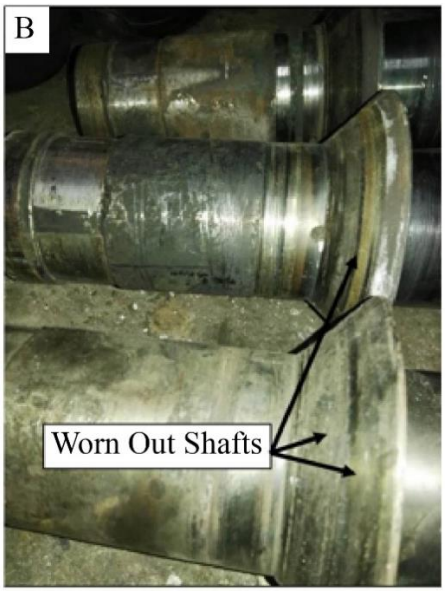

Fig. 10 Observations from industry sites (A) Ruptured AIG seals, and (B) Worn out austenitic stainless-steel shafts.

4. Conclusion

Insights into wear mechanisms and failures of mechanical sealing systems used in the paper industry are obtained. When AIG grade A and C materials rub against grade 304 stainless steel, while subjected to static loading, undergo wear in the steam environment, the wear rate of the composite increases with the increase in contact pressure from 0.36 MPa to 1.12 MPa. After that, it is reduced by an increase in contact pressure. The wear of the stainless-steel material almost ceases once a stable transfer layer is formed in the range of contact pressures from 0.36 MPa to 0.62 MPa. When the contact pressure is increased, a stick-slip regime starts when the progressive wear of stainless steel starts occurring in the zones where the pin directly comes in contact with the disc material without an intermediate protective transfer layer. Above 1.12 MPa contact pressure, aggressive wear of stainless steel commences, reducing the wear rate of AIG material as a significant fraction of the load applied gets utilized in the disc wear. For grade B material, the wear rate was seen as proportional to contact pressures. No aggressive wear of Stainless steel was observed within the range of test parameters for grade B. However, grade B material had undergone frequent fractures during sinusoidal load tests. The fracture propagation was observed to occur through the network of antimony within the composite. For grades A and B, the wear rates observed during sinusoidal loading were less than those during static loads. The excess surface fatigue that occurs during sinusoidal loading may have caused an easier formation of transfer layers. It could also mean the transfer layers have become stable due to a cold working effect. For grade C material, the wear rates during sinusoidal loading were higher than those of the static loading tests.

Data Availability

Data will be made available upon request.

Acknowledgement

The authors would like to gratefully acknowledge the support given by the Department of Technology, Savitribai Phule Pune University, in using their lab facilities.

Author's Contribution

Abhijeet Deshpande was pivotal in identifying the issues at the paper manufacturing sites and in planning in the labs. Lathesh Madhavan converted the site issues into a problem definition under the able guidance of Dr Rahul Waikar. Lathesh, as well as Abhijeet were involved in the testing process.

References

[1] Wang Qi-li, Hu Ya-fei, and He Min, "Effect of Filler on the Self-Lubrication Performance of Graphite Antimony Composites," *Journal of China University of Mining and Technology*, vol. 18, no. 3, pp. 441-443, 2008. [CrossRef] [Google Scholar] [Publisher Link]

[2] Jun Zhao et al., "The Tribological Performance of Metal-/Resin-Impregnated Graphite under Harsh Condition," *Lubricants*, vol. 10, no. 1, pp. 1-13, 2022. [CrossRef] [Google Scholar] [Publisher Link]

[3] H. Zaidi, H. Nery, and D. Paulmier, "Stability of Lubricating Properties of Graphite by the Orientation of the Crystallites in the Presence of Water Vapor," *Applied Surface Science*, vol. 70-71, pp. 180-185, 1993. [CrossRef] [Google Scholar] [Publisher Link]

[4] J.K. Lancaster, "A Review of the Influence of Environmental Humidity and Water on Friction, Lubrication, and Wear," *Tribology International*, vol. 26, no. 6, pp. 371-386, 1990. [CrossRef] [Google Scholar] [Publsher Link]

[5] K. Jradi, M. Schmitt, and S. Bistac, "Surface Modifications Induced by the Friction of Graphites Against Steel," *Applied Surface Science*, vol. 255, no. 7, pp. 4219-4224, 2009. [CrossRef] [Google Scholar] [Publisher Link]

[6] Hozumi Goto, and Kenji Uchijo, "Wear Mechanism of Al-Si Alloy Impregnated Graphite Composite Under Dry Sliding," *Wear*, vol. 259, no. 1- 6, pp. 613-619, 2005. [CrossRef] [Google Scholar] [Publisher Link]

[7] Stephanie Reich, and Christian Thomsen, "Raman Spectroscopy of Graphite," *Philosophical Transactions of the Royal Society a Mathematical, Physical and Engineering Science*, vol. 362, pp. 2271-2288, 2004. [CrossRef] [Google Scholar] [Publisher Link]

[8] Jiang-Bin Wu et al., "Raman Spectroscopy of Graphene-Based Materials and its Applications in Related Devices," *Chemical Society Reviews*, vol. 47, pp. 1822-1873, 2018. [CrossRef] [Google Scholar] [Publisher Link]

[9] Mohammad Asaduzzaman Chowdhury, and Md. Maksud Helali, "The Effect of Amplitude of Vibration on the Coefficient of Friction for Different Materials," *Tribology International*, vol. 41, no. 4, pp. 307-314, 2008. [CrossRef] [Google Scholar] [Publisher Link]

[10] M.A. Chowdhury, and M. Helali, "The Effect of Frequency of Vibration and Humidity on the Coefficient of Friction," *Tribology International*, vol. 39, no. 9, pp. 958-962, 2006. [CrossRef] [Google Scholar] [Publisher Link]

[11] Sudhir Madhav Patil, and B.B. Ahuja, "Effect of Variable Loading Frequency on Wear of PTFE under Dry Sliding Condition Using Novel Variable Loading Wear and Friction Monitor (VLWAFM) Pin-on-disc Sliding Tribometer," *8th International Conference on Industrial Tribology (ICIT 2012)*, pp. 1141-1154, 2012. [Google Scholar]

[12] Sudhir Madhav Patil, and B.B. Ahuja, "Tribological behavior of PTFE under Variable Loading Dry Sliding condition," *Journal of The Institution of Engineers (India): Series C*, vol. 95, no. 2, pp. 179-185, 2014. [CrossRef] [Google Scholar] [Publisher Link]

[13] M. Munakata, M. Tsuji, and S. Kasai, "Occlusal Force Pattern during Rhythmic Human Tapping Movement," *Journal of Oral Rehabilitation*, vol. 18, no. 3, pp. 265-272, 1991. [CrossRef] [Google Scholar] [Publisher Link]

[14] X. Hu et al., "The Influence of Cyclic Loading on the Wear of a Dental Composite," *Biomaterials*, vol. 20, no. 10, pp. 907-912, 1999. [CrossRef] [Google Scholar] [Publisher Link]

[15] Estevam Barbosa de Las Casas et al., "Determination of Tangential And Normal Components of Oral Forces," *Journal of Applied Oral Science*, vol. 15, no. 1, pp. 115–118, 2007. [CrossRef] [Google Scholar] [Publisher Link]

[16] John Fisher, "Wear of Ultra High Molecular Weight Polyethylene in Total Artificial Joints," *Current Orthopaedics*, vol. 8, pp. 164-196, 1994. [CrossRef] [Google Scholar] [Publisher Link]

[17] Feng Li et al., "Influence of Dynamic Load on Friction Behavior of Human Articular Cartilage, Stainless Steel, and Polyvinyl Alcohol Hydrogel as Artificial Cartilage," *Journal of Materials Science: Materials in Medicine*, vol. 21, no. 1, pp. 147-154, 2010. [CrossRef] [Google Scholar] [Publisher Link]

[18] Shashikant S. Goilkar, and Harish Hirani, "Formation of the Transfer Layer and Its Effect on Friction and Wear of Carbon-Graphite Face Seal Under Dry, Water and Steam Environments," *Wear*, vol. 266, no. 11-12, pp. 1141-1154, 2009. [CrossRef] [Google Scholar] [Publisher Link]

[19] Shashikant S. Goilkar, and Harish Hirani, "Parametric Study on Balance Ratio of Mechanical Face Seal in the Steam Environment," *Tribology International*, vol. 43, no. 5-6, pp. 1180-1185, 2010. [CrossRef] [Google Scholar] [Publisher Link]

[20] Shashikant S. Goilkar, and Harish Hirani, "Tribological Characterization of Carbon Graphite Secondary Seal," *Indian Journal of Tribology*, vol. 4, no. 2, pp. 1-6, 2009. [Google Scholar] [Publisher Link]

[21] Shashikant S. Goilkar, and Harish Hirani, "Rotordynamic Analysis of Carbon Graphite Seals of a Steam Rotary Joint," *IUTAM Symposium on Emerging Trends in Rotor Dynamics*, New Delhi, India, pp. 253-262, 2010. [CrossRef] [Google Scholar] [Publisher Link]

[22] K.P. Lijesh, and Harish Hirani, "Thermal Analysis of Floating Ring Mechanical Seal," *International Journal of Thermal Technologies*, vol. 5, no. 1, pp. 28-30, 2015. [Google Scholar] [Publisher Link]